Aerosol optical depths over oceans: A view from MISR retrievals and collocated MAN and AERONET in situ observations

Marcin L. Witek,[1] Michael J. Garay,[1] David J. Diner,[1] and Alexander Smirnov[2]

Received 26 June 2013; revised 17 October 2013; accepted 22 October 2013; published 19 November 2013.

[1] In this study, aerosol optical depths over oceans are analyzed from satellite and surface perspectives. Multiangle Imaging SpectroRadiometer (MISR) aerosol retrievals are investigated and validated primarily against Maritime Aerosol Network (MAN) observations. Furthermore, AErosol RObotic NETwork (AERONET) data from 19 island and coastal sites is incorporated in this study. The 270 MISR/MAN comparison points scattered across all oceans were identified. MISR on average overestimates aerosol optical depths (AODs) by 0.04 as compared to MAN; the correlation coefficient and root-mean-square error are 0.95 and 0.06, respectively. A new screening procedure based on retrieval region characterization is proposed, which is capable of substantially reducing MISR retrieval biases. Over 1000 additional MISR/AERONET comparison points are added to the analysis to confirm the validity of the method. The bias reduction is effective within all AOD ranges. Setting a clear flag fraction threshold to 0.6 reduces the bias to below 0.02, which is close to a typical ground-based measurement uncertainty. Twelve years of MISR data are analyzed with the new screening procedure. The average over ocean AOD is reduced by 0.03, from 0.15 to 0.12. The largest AOD decrease is observed in high latitudes of both hemispheres, regions with climatologically high cloud cover. It is postulated that the screening procedure eliminates spurious retrieval errors associated with cloud contamination and cloud adjacency effects. The proposed filtering method can be used for validating aerosol and chemical transport models.

Citation: Witek, M. L., M. J. Garay, D. J. Diner, and A. Smirnov (2013), Aerosol optical depths over oceans: A view from MISR retrievals and collocated MAN and AERONET in situ observations, *J. Geophys. Res. Atmos.*, *118*, 12,620–12,633, doi:10.1002/2013JD020393.

1. Introduction

[2] Over the past three decades, remote sensing aerosol retrievals from polar orbiting satellites have been a valuable source of information on atmospheric aerosols and pollution. Thanks to these measurements, our understanding of the role atmospheric aerosols play in the climate system have greatly improved, as indicated by subsequent Intergovernmental Panel on Climate Change reports [*IPCC (Intergovernmental Panel on Climate Change)*, 2001, 2007] and many scientific publications. They allowed for detail tracking of aerosol trends [e.g., *Mishchenko et al.*, 2007; *Wild*, 2009] and recognizing their impact on global surface temperature changes and the Earth's energy balance [e.g., *Yu et al.*, 2006; *Quass et al.*, 2008; *Schwartz et al.*, 2010]. Furthermore, the accuracy of satellite-derived aerosol data has greatly improved over time due to enhancements in observational techniques and continuous efforts of various science teams toward refinements of retrieval algorithms.

[3] Despite these evident successes of satellite-based techniques, there is still a substantial variation in the information provided by different satellite platforms such as Advanced Very High Resolution Radiometer, Total Ozone Mapping Spectrometer, Moderate Resolution Imaging Spectroradiometer (MODIS), Multiangle Imaging Spectroradiometer (MISR), Sea-viewing Wide Field-of-view Sensor (SeaWiFS), and others. There have been many studies addressing and explaining these discrepancies [*Lyapustin et al.*, 2007; *Lallart et al.*, 2008; *Liu and Mishchenko*, 2008; *Li et al.*, 2009; *Mishchenko et al.*, 2010; *Zhang and Reid*, 2010; *Kahn et al.*, 2007, 2011; *Shi et al.*, 2011b; *Sayer et al.*, 2012; *Toth et al.*, 2013], some of which are real and some are artifacts of the analysis methodologies. Other research has focused on developing empirical correction and quality assurance techniques that reduce disagreements between satellite and ground-based observations [*Zhang and Reid*, 2006; *Shi et al.*, 2011a]. Further efforts to alleviate the limitations and biases in satellite products are needed to provide accurate assessments of aerosol impacts on climate [*Schwartz et al.*, 2010; *Kahn*, 2012].

[4] Much effort has been devoted to identifying and eliminating sources of errors and discrepancies in aerosol remote sensing from satellites, in particular over oceans. Standard

[1]Jet Propulsion Laboratory, California Institute of Technology, Pasadena, California, USA.
[2]Sigma Space Corporation, Lanham, Maryland, USA.

Corresponding author: M. L. Witek, Jet Propulsion Laboratory, California Institute of Technology, 4800 Oak Grove Drive, Pasadena, CA 91109, USA. (marcin.l.witek@jpl.nasa.gov)

2169-897X/13/10.1002/2013JD020393

retrieval algorithms still suffer from cloud contamination and various cloud adjacency effects [*Zhang et al.*, 2005; *Koren et al.*, 2007; *Remer et al.*, 2008; *Marshak et al.*, 2008; *Várnai and Marshak*, 2009; *Toth et al.*, 2013], which is especially relevant over cloudy circumpolar regions. Possible issues include (a) radiance contamination through inadequate accounting for whitecap coverage and sunglint, in particular over rough oceans [*Zhang and Reid*, 2006; *Shi et al.*, 2011a]; (b) cloud 3-D effects and enhanced Rayleigh scattering [*Kassianov and Ovtchinnikov*, 2008; *Wen et al.*, 2008; *Redemann et al.*, 2009; *Davis and Marshak*, 2010]; (c) aerosol swelling due to increased humidity in the proximity of a cloud [*Twohy et al.*, 2009; *Kassianov et al.*, 2011]; and (d) subvisual and subpixel clouds, cirrus in particular. Some issues have been partially addressed in recent revisions of retrieval algorithms, for example, by better characterization of the lower boundary conditions (wind speed and whitecap coverage). Other studies demonstrated that more rigorous screening and correction procedures applied to MODIS aerosol product eliminate many aerosol optical depth (AOD) outliers and reduce the magnitude of the over ocean AODs [*Zhang and Reid*, 2006, 2010; *Shi et al.*, 2011a; *Sayer et al.*, 2012]. However, "twilight zone" [*Koren et al.*, 2007] and cloud adjacency contaminations still persist and remain largely unaccounted for in standard aerosol products [*Kassianov et al.*, 2011]. Fortunately, studies that address these issues are aided by the increasing availability of surface-based active and passive observations, including measurements carried out in remote oceanic regions.

[5] Satellite aerosol retrievals are commonly validated against surface based AERosol RObotic NETwork (AERONET) Sun photometer observations [*Holben et al.*, 1998]. Relatively recently the AERONET network was expanded to include measurements performed from ships and integrated within the Maritime Aerosol Network (MAN) [*Smirnov et al.*, 2009, 2011]. The MAN observations complement traditional land- and island-based AERONET measurements with data collected over open oceans using observations made by hand-held Sun photometers onboard ships. MAN started operating in November 2006 and the database continues to grow, sampling many areas of the world's oceans. These measurements are valuable for validating satellite aerosol retrievals. They increase geographical coverage for comparison studies by bringing in atmospheric observations in remote locations of the world, and they provide observations unaffected by nearby islands and continents. The MAN data set has already been used for assessing the quality of satellite retrievals [*Kahn et al.*, 2010; *Smirnov et al.*, 2011; *Sayer et al.*, 2012; *Toth et al.*, 2013] as well as aerosol transport model simulations [*Smirnov et al.*, 2011]. A study by *Kahn et al.* [2010] found about 60 MISR/MAN coincident comparison points. More recent studies by *Smirnov et al.* [2011] and *Sayer et al.* [2012] found substantially more collocations, which was primarily due to better coverage of satellite data they used (MODIS and SeaWiFS, respectively). *Toth et al.* [2013] found almost 200 MAN/MODIS Aqua collocations over the Southern Ocean.

[6] In this study, we use MAN and AERONET data sets to investigate the accuracy of MISR over ocean aerosol retrievals. We focus particularly on the MAN data set, taking advantage of an increased number of MISR/MAN collocations. Additional island and coastal AERONET stations complement our analysis by further improving the statistics. The paper is organized as follows. Section 2 describes data sets and methodology used in this study. Section 3 forms the main body of this manuscript. It presents the initial MISR/MAN comparison results, introduces a new data screening procedure, validates MISR AODs against combined MAN and AERONET AODs, and analyzes a global 12 year climatology of MISR over ocean retrievals. In section 4 the physical basis of the newly proposed bias-reducing procedure is discussed. Finally, section 5 summarizes the study.

2. Methodology

2.1. MISR Retrievals

[7] The Multiangle Imaging SpectroRadiometer (MISR) instrument, launched aboard NASA's Terra satellite, has been collecting global data since February 2000. Terra's descending, sun-synchronous polar orbit crosses the equator around 10:30 A.M. local time. MISR consists of nine pushbroom cameras with the viewing angles of 0º (nadir), ±26.1°, ±45.6°, ±60.0°, and ±70.5° along the flight track. Each camera measures reflected shortwave radiance in four spectral bands, centered at 446, 558, 672, and 866 nm. Within a 7 min time interval the cameras see a 380 km wide overlap swath from all nine angles. This typically allows a large range of scattering angles to be sampled leading to a better characterization of aerosol optical properties. Near-global coverage (except for latitudes poleward of ±82°) is obtained within 9 days, and high latitudes have more frequent sampling than the tropics.

[8] The spatial resolution of the operational MISR aerosol retrieval algorithm is 17.6 km × 17.6 km. The retrieval region consists of 16 × 16 subregions, each covering a 1.1 km × 1.1 km area. A sophisticated quality control and cloud screening procedure is applied to each subregion to determine its applicability for aerosol retrievals [*Kahn et al.*, 2009]; a detailed description of these procedures is provided in the appendix. For ocean surfaces, retrievals are attempted if at least 32 out of 256 subregions are designated as usable across at least four cameras. The red (672 nm) and near-infrared (866 nm) bands are used primarily for aerosol retrieval. In the green (558 nm) and blue (446 nm) channels, surface reflectance is nonnegligible. However, when AOD is over 0.5 then the green band is included in the minimization procedure, and if AOD exceeds 0.75 the blue channel is additionally incorporated. This is because as the AOD increases, the relative surface contribution to the overall equivalent reflectances lessens. From subregions that qualify for retrieval, the one that is darkest is chosen for further processing. As a result, the exact 1.1 km × 1.1 km location of the retrieval is identified. This procedure is different from other satellite instruments. In MODIS retrievals, for example, radiances from 50% qualifying subregions are averaged and the retrieval is performed on these average values (subregions from the lowest and highest quartile of the radiance distribution are excluded, *Remer et al.* [2005]). Despite different methodologies, the MISR and MODIS reported radiances that are used for aerosol retrievals agree with each other very well [*Kahn et al.*, 2005b, 2007; *Lallart et al.*, 2008]. The quality of the MISR aerosol retrieval product has been documented in many publications

Table 1. AERONET Validation Sites Used in This Study[a]

Site Name	Latitude (N)	Longitude (E)	Elevation (m)	Coincidence Count
Amsterdam Island	□37.81	77.57	30	25
Ascension Island	□7.98	□14.41	30	97
Appledore Island	42.99	70.61	35	42
Azores	38.53	□28.63	50	35
Barrow	71.31	156.66	0	38
Bermuda	32.37	□64.70	10	45
Coconut Island	21.43	□157.79	0	41
Graciosa	39.09	28.03	15	32
Ittoqqortoormiit	70.48	□21.95	68	19
Lanai	20.73	□156.92	20	102
Midway Island	28.21	□177.38	20	92
Nauru	□0.52	166.92	7	126
Prospect Hill	32.37	□64.70	63	28
Reunion St Denis	□20.88	55.48	0	124
Rottnest Island	□32.00	115.50	70	60
Sable Island	43.93	□60.01	3	14
Sagres	37.05	8.87	26	30
Tahiti	□17.58	□149.61	98	71
Tudor Hill	39.26	64.88	51	74

[a]The last column, coincident count, is the number of collocated MISR/AERONET observations.

[*Martonchik et al.*, 2004; *Kahn et al.*, 2005a, 2005b, 2007, 2009, 2010, 2011; *Dey and Di Girolamo*, 2010]. In this study, we use MISR's Dark Water best estimate AOD retrievals as reported in RegBestEstimateSpectralOptDepth field in the MISR V22 product.

2.2. Maritime Aerosol Network (MAN) Observations

[9] The Maritime Aerosol Network [*Smirnov et al.*, 2006, 2009, 2011] has been collecting data over the oceans since November 2006. The network deploys handheld Microtops II Sun photometers with five spectral channels within the 340–1020 nm range. Calibration and data processing procedures are similar to those employed within the AERONET network [*Holben et al.*, 1998, 2001; *Smirnov et al.*, 2004]. The estimated uncertainty of the postfield calibrated optical depth is less than ±0.02 in each channel [*Knobelspiesse et al.*, 2004]. However, *Porter et al.* [2001] suggested that the error could be higher (on average ±0.025) due to the increased difficulties in pointing at the Sun on an unstable ship platform.

[10] In this study, we use MAN Level 2.0 (cloud screened and quality assured) data from 180 cruises. We obtained the data set in October 2012 and analyzed 17,787 over ocean AOD observations (Level 2, individual series) and 3089 measurement days. As the MAN database keeps growing, more cruises and open ocean measurements will be available for satellite intercomparisons in the future.

2.3. Aerosol Robotic Network (AERONET) Observations

[11] AERONET is a ground-based Cimel Sun photometer aerosol monitoring network [*Holben et al.*, 1998, 2001]. Direct Sun measurements are taken at eight spectral bands, between 340 and 1020 nm wavelength (440, 670, 870, 940, and 1020 nm are standard). The instruments are intercalibrated with reference Cimel instruments, typically at the NASA Goddard Space Flight Center, which are in turn calibrated at Mauna Loa Observatory in Hawaii using the Langley method. The data accuracy for AOD is very high, with the uncertainty between ±0.01–0.02 for wavelengths higher than 440 nm [*Holben et al.*, 1998].

[12] In this study, we use V2 AERONET Level 2.0 data, which has additional postdeployment calibration and manual validation checks. We choose 19 AERONET sites (see Table 1 for details) for which MISR has at least ten coincident dark water aerosol retrievals. They are generally maritime sites, mostly in remote oceans and several coastal locations. Many sites are the same as in previous MISR comparison studies [*Kahn et al.*, 2005a, 2010]. We added a few additional island locations not used in previous reports.

2.4. Collocation Procedure

[13] In order to find coincident ground-based and satellite observations, we perform spatial and temporal matching of the data. Our criteria differ slightly between MISR/MAN and MISR/AERONET points. Since MAN measurements often change location while the ship is cruising, we allow for a broader perimeter around the central location and longer time window for potential MISR overpasses. We look for MISR overpasses within ±1 h of the MAN observation and localize successful MISR retrievals in a 30 km radius around the MAN location. Since the MISR aerosol retrievals are reported at a spatial resolution of 17.6 km × 17.6 km, this gives on average nine retrieval regions per collocation. This procedure differs somewhat from previously used spatial collocation [*Kahn et al.*, 2005a, 2007, 2010], which identifies the closest MISR region and takes the central one plus eight surrounding regions into consideration. Although we found both approaches conceptually comparable (in particular for radius 30 km, which gives on average nine regions), our method allows for more flexibility in terms of specifying the distance and perimeter around the MAN location.

[14] The MISR/AERONET collocation criteria are more stringent, with the time window ±45 min around the MISR overpass and the distance 25 km from the AERONET location. The matching is successful if there is at least one AERONET observation in this time frame and one successful MISR retrieval within the perimeter.

[15] MISR retrieves AODs at four spectral bands that do not correspond to the nominal MAN and AERONET wavelengths. To facilitate comparisons, we interpolated Sun photometer data to MISR's green band (558 nm) using a linear fit in the ln

Table 2. Summary of MISR/MAN and MISR/AERONET Collocation Criteria

	MISR/MAN	MISR/AERONET
MISR Perimeter	30 km	25 km
Time Interval	± 1 h	± 45 min
Number of Collocations	270	1095

(AOD) versus ln(wavelength) space. Some other studies recommend using a second-order polynomial [*Eck et al.*, 1999; *Kahn et al.*, 2010]. We explored this option but found the linear fit generally more suitable (results not shown). This could be due to the fact that MAN observations have, on average, fewer wavelengths than AERONET, which in some cases makes a second-order polynomial vary too much between wavelengths, rendering the linear fit a more suitable approach.

[16] Table 2 summarizes the collocation criteria and results for the MISR/MAN and MISR/AERONET data sets. We found 270 MISR/MAN and 1095 MISR/AERONET comparison points.

[17] The new comparison data set, in particular the MISR/MAN collocations, is valuable for assessing MISR dark water retrievals. For comparison, the previous studies by *Kahn et al.* [2010] and *Smirnov et al.* [2011] used only 61 and 54 MISR/MAN collocations, respectively, which limited any extensive statistical analysis of these cases. Here the open ocean MISR/MAN comparison data set is sufficiently large to enable detailed analysis. These collocations are geographically diverse and allow for verification of satellite retrievals in remote, previously unexamined regions. Potential issues relevant to island AERONET AOD retrievals such as the influence of surf zone, shallow water, and wind blocking on the lee side of the islands are also alleviated with the MAN observations.

3. Results and Analysis

3.1. MISR Versus MAN

[18] As noted above, the collocation procedure found 270 MISR/MAN comparison points. Their geographical distribution is presented in Figure 1, with the color code showing the AOD difference (MISR-MAN) for each collocation. The data set covers all of the world's oceans [*Smirnov et al.*, 2011], although the Atlantic Ocean has the biggest representation in our data set. Some collocations are present in the Southern Ocean for which satellite retrievals have been particularly challenging because of high cloud coverage [*Zhang and Reid*, 2010]. Many points are located next to Antarctica in somewhat sheltered waters; MAN AODs are typically very low there.

[19] Figure 2 shows scatter plots for MISR/MAN collocations (Figures 2a and 2b, linear and log-log scale) as well as AOD difference as a function of latitude (Figure 2c) and a histogram of the difference (Figure 2d). On average, MISR overestimates AODs compared to MAN by 0.043. This is especially evident in the low-to-medium AOD range, where the log-log scatter plot shows a clear deviation from the one-to-one line. For higher AODs, the agreement is very good, although a slight high bias is apparent. We did not find any evident latitudinal patterns in the AOD differences (Figure 2c). Some MISR underestimations are observed in the Bay of Bengal, tropical Atlantic off the coast of Africa, and off the coast of Europe (Figure 1); all such cases are associated with relatively polluted scenes. Almost all MISR retrievals from close to Antarctica are grossly overestimated, which introduces substantial relative errors given the typically low AOD values found there. A histogram of the AOD difference peaks to the right of the zero line and is positively skewed, indicating that MISR overestimations are more frequent and larger than MISR underestimations. Some basic details of the statistics are presented in Table 3. It is worth mentioning that in terms of correlation and RMSE, our MISR/MAN data set compares favorably to other similar satellite validation efforts. For example, SeaWiFS over ocean comparison with AERONET indicates correlation of up to 0.89 when the highest quality product is used [*Sayer et al.*, 2012]. A comprehensive MODIS Terra and Aqua over ocean comparison with AERONET reveals correlations of 0.903 and 0.907, respectively [*Remer et al.*, 2008]. *Shi et al.* [2011a] found the RMSE between MODIS and AERONET AOD to be 0.092 for Terra and 0.087 for Aqua. After their sophisticated quality assurance and empirical correction

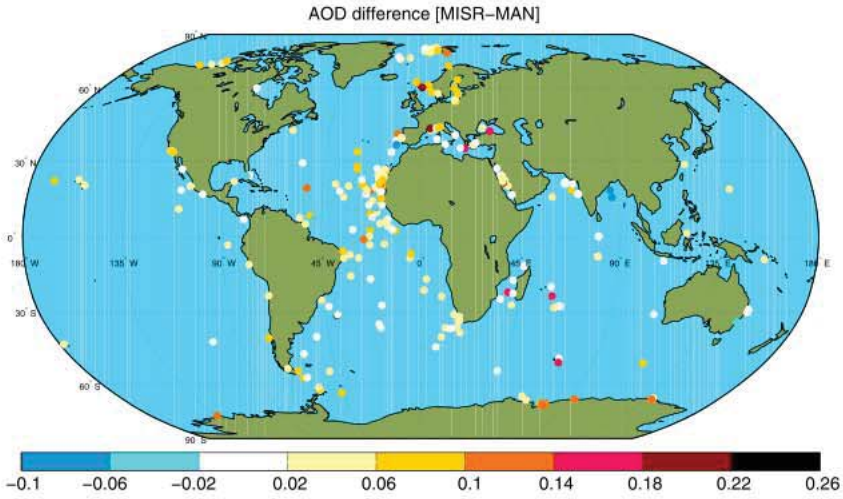

Figure 1. Geographical distribution of MISR/MAN collocations. The color scale represents AOD difference between MISR and MAN.

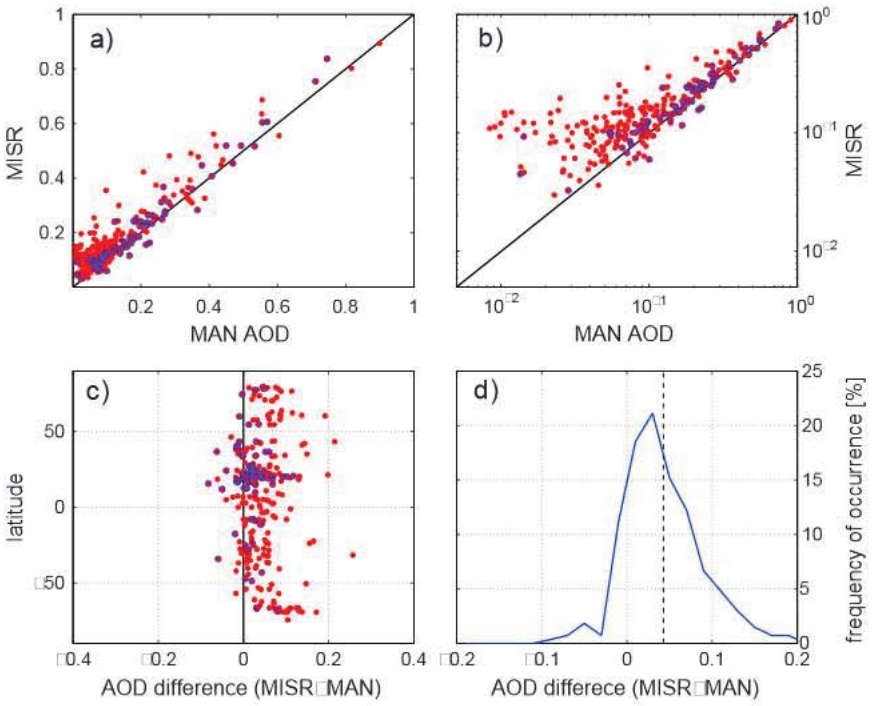

Figure 2. (a) and (b): scatter plot of MISR/MAN collocations (c) MISR-MAN AOD difference as a function of latitude (d) histogram of MISR-MAN AOD difference (the vertical line represents the mean value). The points with blue borders are for CFF > 0.6 (see section 3.2 for details).

procedures, these RMSEs decreased to 0.061 and 0.069 for Terra and Aqua, respectively. Those MODIS validation studies, however, were based on substantially larger and more robust comparison data sets, which could somehow explain less favorable statistics. Overall, our MISR/MAN collocated database corroborates previous validations of the high quality of MISR aerosol retrievals over ocean.

[20] Another way to look at satellite retrieval accuracy is to investigate differences as a function of ground-based AODs, which are taken to represent the "truth". This approach is reflected in aerosol retrieval quality statements that present agreement as both a relative and absolute agreement with AERONET [see *Kahn et al.*, 2011]. Figure 3 shows the MISR-MAN AOD differences as a function of MAN AODs. Over 62% of MISR retrievals fall within the larger of 0.05 or 20% AOD envelope. This frequency of occurrence is smaller than the value of 70–75% reported by *Kahn et al.* [2010] for all MISR/AERONET dark water retrievals but is based on a different comparison data set. Our result can be ascribed to a combination of two factors: a fairly low median value of MAN AODs in collocated points (= 0.09), and a higher MISR bias for low optical depths. Indeed, the MISR bias for points with MAN AODs lower than 0.1 approaches 0.05, whereas for points with AODs higher than 0.1 the corresponding MISR bias is 0.03. With more comparison points being fairly pristine (57% of AODs are smaller than < 0.1), the 0.05 accuracy threshold is exceeded more often. This frequent overestimation of MISR retrievals has been recognized in previous studies [*Kahn et al.*, 2009, 2010]. An apparent gap in MISR-retrieved AODs below about 0.02 was also identified, but no culprit or solution has been previously identified. *Kahn et al.* [2009, 2010] also found quantization noise in the reported MISR AODs at intervals of 0.025, which becomes evident at very low AODs. This has since been attributed to an idiosyncrasy of the procedure used to interpolate AOD in the retrieval grid, which will be corrected in the next product release. Here we investigate another likely factor affecting over ocean MISR retrievals: contamination of the retrieval scene by clouds and other artifacts. Our aim is to remove or substantially reduce the observed biases to increase confidence of MISR-derived aerosol climatology over oceans.

Table 3. Basic Statistics of MISR/MAN and MISR/AERONET Comparison Data Sets[a]

	MISR/MAN		MISR/AERONET	
	All Points	CFF > 0.6	All Points	CFF > 0.6
MISR Average	0.186	0.236	0.125	0.111
Sun photometer Average	0.143	0.218	0.090	0.090
R	0.946	0.977	0.804	0.855
RMSE	0.064	0.041	0.055	0.039
Number of Collocations	270	61	1095	149

[a]*R* is the correlation coefficient; RMSE is root-mean-square error. The values in parentheses are statistics for a subset of points with clear flag fraction (CFF) > 0.6 (see section 3.2 for details).

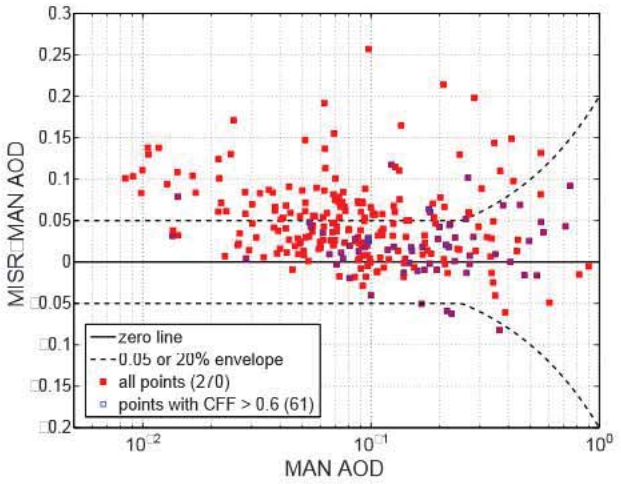

Figure 3. MISR-MAN AOD difference plot as a function of MAN AOD. The points with blue borders are for CFF > 0.6 (see section 3.2 for details).

3.2. Retrieval Region Analysis

[21] As mentioned in section 2.1, MISR reports aerosol retrievals within 17.6 km × 17.6 km regions. The retrieval region consists of 16 × 16 subregions, each 1.1 km × 1.1 km in size. Each subregion is checked individually for its suitability for aerosol retrieval. The process of quality control assigns a flag to a subregion to indicate whether it is "clear" and appropriate for further aerosol retrievals, or otherwise contaminated and unsuitable for retrieval. There are about 16 quality flags stored in the Retrieval Applicability Mask (RetrAppMask) field in the MISR Level 2 aerosol product and described in detail in the Data Products Specifications manual [*MISR Data Product Speci□cation*, 2011; see also *Kahn et al.*, 2009]. Furthermore, each subregion is observed by nine MISR cameras. This gives in total 16 × 16 × 9 = 2304 quality flags for a single AOD retrieval region, as schematically depicted in Figure 4. We use this subscale information to investigate retrieval region characteristics and look for additional indicators of MISR retrieval quality. In particular, we investigate MISR/MAN discrepancies in terms of retrieval scene variability, as indicated by the Retrieval Applicability Mask flags.

[22] Figure 5 shows the MISR-MAN difference as a function of the fraction of clear flags in the region. The fraction is computed by dividing the number of subregion flags marked as clear by the total number of flags, namely by 2304. The data points are scattered considerably, but a decreasing trend is apparent. The higher the fraction of clear flags in the region, the smaller the bias in MISR AOD retrievals relative to the MAN data. If we consider only points with the clear flag fraction (CFF) higher than 0.6, the bias decreases from 0.043 to 0.018; it reaches zero for CFF above 0.85.

[23] Figure 5 demonstrates a simple analysis that is able to substantially reduce, or even remove, the MISR bias relative to the MAN observations described previously. One unwanted consequence of such a procedure is decreased coverage as more MISR retrievals are excluded with higher CFFs. For higher CFFs, we reach a point where statistical significance of the results becomes an issue. For example, the bias approaches zero for CFF > 0.85, but the number of comparison points drops down to 6. For CFF > 0.6, there are over 60 comparison points, which is about 77% reduction from the original pool of data. Although the 270 MISR/MAN comparison points appears statistically sound, the number of data for higher CFF decreases considerably (see the inset in Figure 5). To increase the statistical significance of our results we added land-based AERONET stations in our analysis. Results of the combined MAN and AERONET versus MISR collocations are presented in the next section.

[24] The correlation coefficient for the MISR-MAN regression versus CFF is □0.43. We also investigated possible correlations with other 16 Retrieval Applicability Masks. We found meaningful regressions only with the fraction of cloudy flags (R = 0.29) and glitter-contaminated flags (R = 0.24). However, those were less significant than the CFF (R = □0.43); therefore, we did not pursue further analysis of those metrics.

3.3. MISR Versus Combined MAN and AERONET

[25] Including 19 AERONET stations adds 1095 comparison points. Along with the MISR/MAN collocations, the combined data set consists of 1365 points. Figure 6 presents the difference between MISR and the combined observations as a function of CFF. The linear regression for the MISR/AERONET collocations is slightly weaker than that of MISR/MAN. The correlation coefficients are □0.3, □0.43, and □0.33 for MISR/AERONET, MISR/MAN, and MISR/OBS, where OBS is a full 1365 set of collocated observations (AERONET + MAN). By excluding points with low CFFs the MISR-OBS positive bias gradually decreases from

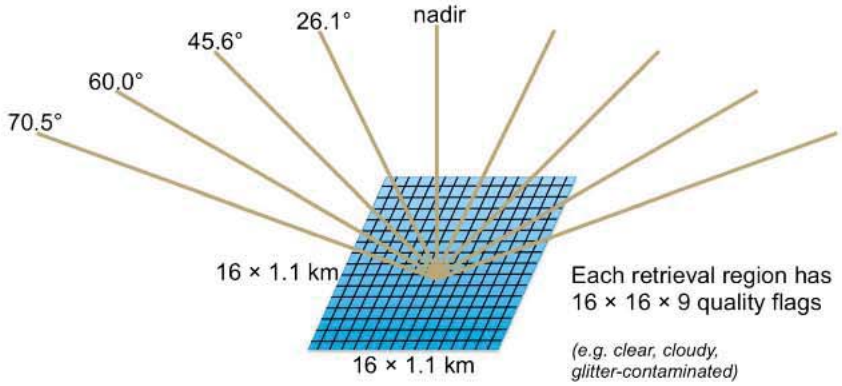

Figure 4. Conceptual representation of MISR viewing geometry (nine angles) and MISR retrieval region.

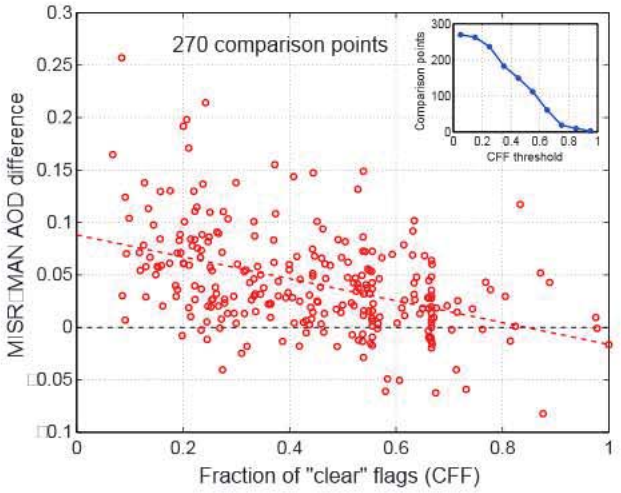

Figure 5. AOD difference between MISR and MAN as a function of CFF (the fraction of clear flags in the region, see text for details). The dashed red line represents a linear regression of the data: DIFF = 0.088–0.104 × AOD, with the correlation coefficient $R = \square 0.43$. The inset shows the number of comparison points with CFF higher than a particular CFF threshold.

its initial value of 0.036—for CFF > 0.6 the bias is 0.02. It decreases even further for higher CFF, but the trend also becomes noisier due to the lower number of available points. For CFF > 0.6, there are still over 200 points included in the comparison, or about 15% of the total data set.

[26] We further examine the trends from Figure 6 with respect to certain AOD ranges. This is to make sure our bias reduction procedure is not specific to more polluted or hazier scenes. Figure 7 shows MISR-OBS differences as a function of CFF for AOD ranges of 0–0.05, 0.05–0.2, and > 0.2 (Figures 7a–7c). The selection was done with respect to the observation AODs. The corresponding linear regressions are also plotted. Figure 7d shows all the collocated points and three regression lines for comparison. Table 4 displays basic statistics and fitting coefficients for the analyzed AOD ranges.

[27] The MISR AOD bias relative to the observations shows decreasing trends in all examined AOD regimes. Linear fits to the data show the slope for the whole data set is □ 0.08; the individual groups vary from □ 0.07 to □ 0.1. The correlation coefficients range from □ 0.42 to □ 0.24, with the overall coefficient for all points equal □ 0.33. Large scatter of MISR/OBS comparison points contributes to relatively low values of correlation coefficients. This is expected, as the root-mean-squared error of MISR-OBS is larger than the bias itself. There are also no obvious reasons that the standard deviation for points with higher CFF should be lower than for points with smaller CFF. Indeed, visual inspection of Figure 7d indicates a fairly even scatter of points around the mean for a broad range of CFFs. More quantitatively, the standard deviation does not change considerably in the 0.2–0.8 CFF range and stays a bit above the overall bias (results not shown). Despite this considerable scatter, filtering out MISR retrievals with low CFF reduces the bias with respect to MAN and AERONET regardless of actual aerosol content. This result gives us confidence that even for low maritime AOD scenarios the CFF filtering procedure effectively reduces biases in MISR retrievals relative to the observations.

3.4. Global Over Oceans AOD Distribution

[28] The screening procedure that reduces MISR retrieval bias is now applied to 12 years of MISR maritime aerosol data. This is to illustrate a potential use of the method and assess its performance on a global scale. Retrievals are binned into 1° × 1° boxes. The clear flag fraction is calculated for each AOD retrieval, and only points with CFF values higher than a certain threshold are considered. In this investigation, we choose the threshold CFF to be 0.6. Such a selection lowers the MISR/MAN bias from 0.043 to 0.018, MISR/AERONET bias from 0.035 to 0.021, and the overall combined bias (MISR/OBS) from 0.036 to 0.02. Increasing the CFF threshold could further reduce the remaining errors; however, the current choice represents a necessary and—in our opinion—balanced compromise between the bias reduction and the statistics of remaining points. In some oceanic regions, the CFF is consistently low due to persistent cloudiness. Setting the CFF threshold higher than 0.6 drastically decreases coverage in such areas. In order to maintain a consistent global analysis, a certain level of bias is therefore unavoidable. It is worth mentioning, however, that the remaining bias is comparable with the ground-based observational uncertainties, which are ±0.02 AOD for the MAN data set [*Smirnov et al.*, 2011].

[29] Figure 8 shows a global average over-ocean AOD distribution obtained from 12 years of MISR retrievals. Figure 8a presents all valid retrievals; Figure 8b shows retrievals with CFF higher than the threshold; and Figure 8c shows the difference between the two. A quick look reveals the typical distribution of AOD, with highest values west of Africa (mineral dust, biomass burning), around Middle East and Asia (mineral dust, anthropogenic) and Indonesia (biomass burning). Elevated AOD values are also found in remote oceanic regions, like the Southern Ocean and North

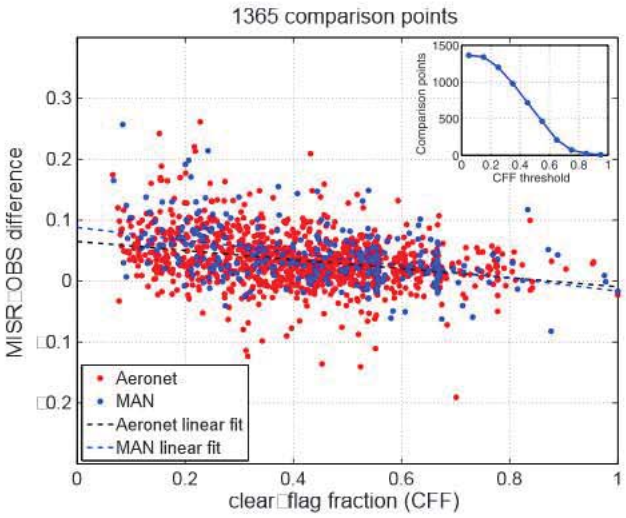

Figure 6. AOD difference between MISR and OBS (MAN + AERONET) as a function of CFF (clear flag fraction in the region, see text for details). The dashed black and blue lines represent linear regressions of the data: DIFF = 0.088–0.104 × AOD (for MAN) and DIFF = 0.065–0.074 × AOD (for AERONET) with the correlation coefficient $R = \square 0.43$ and $R = \square 0.30$ for MAN and AERONET, respectively. The inset shows the number of comparison points with CFF higher than a particular CFF threshold.

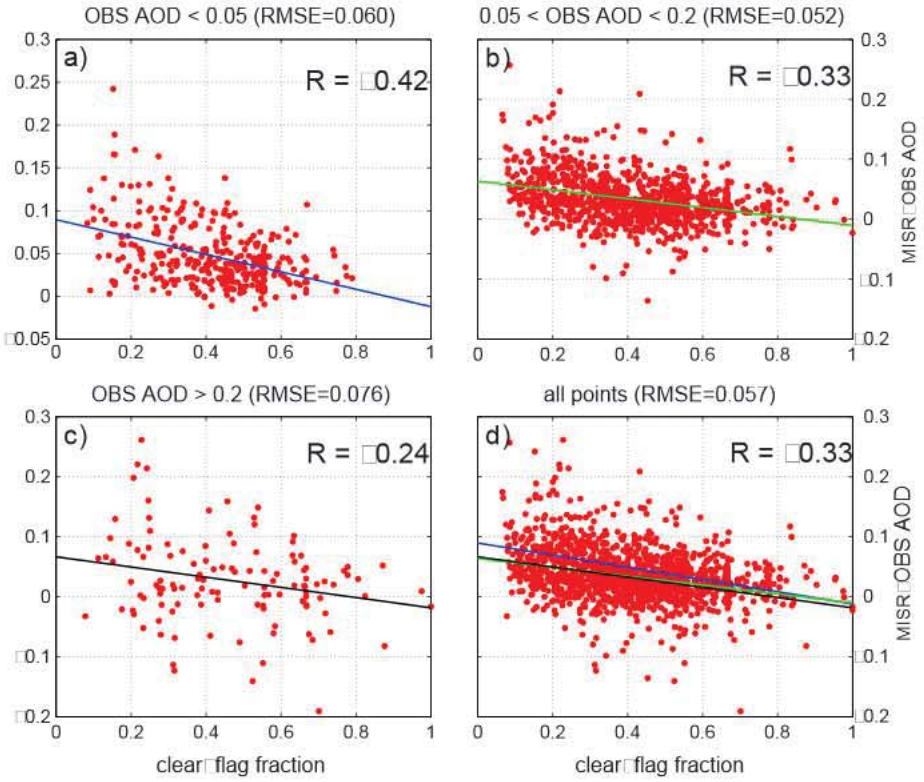

Figure 7. AOD difference between MISR and OBS (MAN + AERONET) as a function of CFF (clear flag fraction in the region, see text for details) grouped into three AOD ranges (low, medium, and high) with respect to ground-based observations: (a) AOD < 0.05; (b) AOD > 0.05 and AOD < 0.2; and (c) AOD > 0.2. (d) all points and corresponding regression lines from three other panels for comparison. On top of each panel the root-mean-square error (RMSE) of MISR-OBS for specific AOD ranges is provided.

Atlantic, away from anthropogenic and land-based aerosol sources. In these supposedly clean oceanic areas, the AOD is substantially reduced after applying the CFF filtering procedure. Generally, we observe AOD reduction over most oceans, as evidenced in Figures 8b and 8c. The largest differences coincide with regions of high cloudiness, like those with stratocumulus clouds, midlatitude storm tracks, and deep convection. Of particular relevance is the already mentioned strong AOD reduction over the Southern Ocean, with local changes exceeding 0.1. This result is in qualitative agreement with the recent study by *Toth et al.* [2013] who found 30–40% reduction in MODIS derived AODs over the Southern Ocean after applying additional cloud screening using the Cloud-Aerosol Lidar with Orthogonal Polarization data. Nevertheless, elevated aerosol concentrations are still present in the Southern Ocean (Figure 8b), which is in accord with the expected increase in sea salt aerosol concentrations due to strong surface winds [e.g. *De Leeuw et al.*, 2011].

[30] The difference map also shows some areas where AOD slightly increases after CFF masking. Those are primarily regions dominated by mineral dust aerosol, and the increase usually does not exceed 0.02 (less than 1% of all points have an AOD increase larger than 0.02). These upward AOD corrections are not obvious to interpret. An additional analysis reveals that they do not result from decreased retrieval statistics in those areas (results not shown). The CFF filtering is a bias adjustment procedure relative to the observations, and as such it does not always guarantee AOD reduction. The mean bias is adjusted downward, but locally the CFF screening can lead to AOD increase, as evident in Figure 8c.

[31] Figure 9 presents the zonally averaged latitudinal distribution of AOD over oceans for the standard V22 MISR retrievals and for the CFF-screened data. The difference between the two is plotted with the dashed line. The highest AOD reduction (~0.05) is in the high latitudes of the Southern and Northern Hemispheres, and the smallest is in

Table 4. Analysis of MISR/OBS Collocations for Specific AOD Ranges (Relative to OBS)[a]

		MISR-OBS (y) Versus CFF (x) Trends	
OBS AOD range	OBS/MISR RMSE	Linear Regression	Correlation Coefficient
0–0.05	0.060	$y = -0.10x + 0.09$	−0.42
0.05–0.2	0.052	$y = -0.07x + 0.06$	−0.33
0.2–5	0.076	$y = -0.08x + 0.07$	−0.24
0–5 (All Data)	0.057	$y = -0.08x + 0.07$	−0.33

[a]OBS/MISR RMSE is the root-mean-square error. A first-order polynomial is fitted to the MISR-OBS difference as a function of CFF: Linear regression and correlation coefficient are shown. CFF stands for clear flag fraction (see section 3.2 for details).

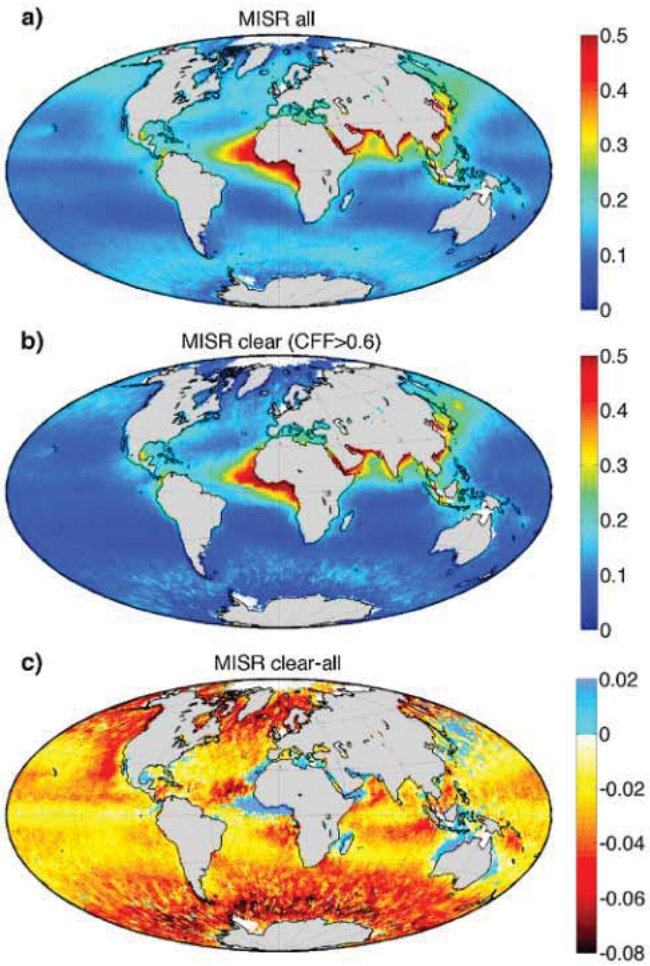

Figure 8. Average AOD distribution over oceans based on 12 years of MISR retrievals. (a) All valid MISR retrievals; (b) subset of MISR retrievals with clear flag fraction higher than 0.6; and (c) difference between Figure 8b and 8c.

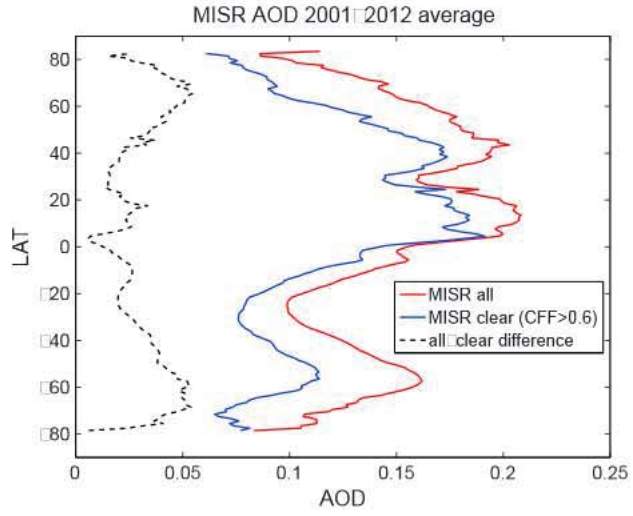

Figure 9. Longitudinally averaged AOD over ocean based on 12 years of MISR retrievals. Red line is for all MISR retrievals; blue line is for a subset of retrievals with clear flag fraction higher than 0.6, and dashed black line is the difference between the two.

the Tropics (~0.01). A pronounced decrease of the peak in the Southern Ocean is evident here, but the local maximum is still observed. Globally, the multiannual average AOD changes from 0.149 to 0.119, a decrease by 0.03. This is a substantial change from the radiative transfer and energy balance point of view. It could also have an impact on our assessments of aerosol influence on clouds, since the highest AOD reductions are observed in typically cloudy regions. A similar AOD decrease, but for the MODIS data, was obtained by *Zhang and Reid* [2010] after their extensive quality assurance procedures and empirical corrections applied to retrieved AODs. Their globally averaged over-ocean MODIS Level 3 data assimilation quality AOD is lower by ~0.035 for MODIS Terra and ~0.03 for MODIS Aqua, as compared to the original Level 2 products (~20–30% reduction). The similar outcomes, despite different screening procedures, might be coincidental, but also might point to a common physical rationale for such methods. They suggest that cloud contamination in the state-of-the-art passive remote sensing contributes to AOD by at least 0.03, on average.

[32] The 0.03 decrease in the MISR over ocean AOD, however, is still within a range of values obtained from various satellite platforms. For comparison, the multiannual

global mean AOD at 550 nm over oceans from MODIS Collection 5 product is 0.13 for Aqua and 0.14 for Terra [*Remer et al*., 2008]. For SeaWiFS over ocean AODs, *Sayer et al*. [2012] do not report a corresponding multiannual mean, but the difference in daily average AOD for collocated SeaWiFS and MISR retrievals is □ 0.036, MISR being larger. These various assessments should increase users' awareness of strengths and limitations of different satellite data sets and also motivate further studies aimed at providing a realistic unified data set.

4. Discussion

[33] The previous section provided evidence that the screening procedure based on a fraction of clear flags in the region reduces MISR AOD retrieval biases with respect to ground-based MAN and AERONET observations. So far, we refrained from giving any physical interpretation for our findings. Here we briefly elaborate on possible reasons why such a procedure works and on physical mechanisms contributing to the presence of bias in the first place.

[34] Even a cursory visual inspection of satellite AOD maps often indicates an increase of AOD in the proximity of clouds. This effect has been broadly recognized [*Zhang et al*., 2005; *Koren et al*., 2007; *Marshak et al*., 2008; *Redemann et al*., 2009; *Várnai and Marshak*, 2011]; it has been often described in terms of strong correlation between AOD (or clear-sky reflectance) and cloud cover. Many researchers have analyzed this phenomenon, providing physical description and quantitative assessments of this effect. Generally, existing explanations fall into three categories: (1) aerosol properties and composition change in the proximity of clouds due to various reasons, (2) satellite retrievals are directly contaminated by clouds, and (3) satellite observations suffer from cloud adjacency (or three-dimensional) effects. The third category mostly concerns passive satellite retrievals. It is worth mentioning that the majority of studies analyzing satellite retrievals used MODIS observations. Very little discussion was focused on other satellite platforms, in particular on MISR retrievals. Although conclusions based on MODIS data are general enough, the specifics might be different for other instruments.

[35] The first category listed above concerns spatial and temporal changes in aerosols in the proximity of clouds. The aerosol composition, size distribution, and concentration can be modified in the vicinity of clouds due to changes in relative humidity, cloud processing, and nucleation of new particles [*Su et al*., 2008; *Twohy et al*., 2009; *Jeong and Li*, 2010; *Kassianov et al*., 2011]. Subsequently, these modifications impact aerosol optical properties and the resulting AOD. For example, *Su et al*. [2008] assessed—using high spectral resolution lidar—that AOD is about 8 to 17% higher in the proximity of clouds, which they attributed to aerosol swelling due to higher relative humidity and to aerosol growth through in-cloud processing. *Koren et al*. [2007] found a 13% ± 2% increase in the visible AOD close to the clouds based on AERONET observations. Other studies have found the influence of humidification to be somehow larger [*Twohy et al*., 2009; *Jeong and Li*, 2010]. Nonetheless, if MAN/AERONET and MISR instruments have observed the same scene, they should be looking at the same aerosols, regardless of whether they are close to or processed by clouds. Such precise collocation is very difficult to achieve; in addition, the Sun photometers view the aerosols present along the line of sight to the Sun, whereas MISR sees aerosols within slanted columns not oriented with the solar azimuth. Therefore, some variability in the results is to be expected. However, it seems likely that such variability would be random, rather than contributing to a bias.

[36] Another explanation for AOD increasing with cloud fraction is direct contamination by clouds. The premise is that radiances measured by satellite instruments can be affected by subvisual thin cirrus clouds or subpixel clouds [*Kaufman et al*., 2005; *Zhao et al*., 2009; *Toth et al*., 2013]. Such cloud contaminations are sometimes undetected by various cloud-screening procedures employed. *Kaufman et al*. [2005] estimated the cloud contamination impact on MODIS AOD to be around 0.02, of which 0.015 is due to residual cirrus. *Toth et al*. [2013], on the other hand, argue that stratocumulus and low broken cumulus clouds contaminate AOD retrievals over the Southern Ocean, leading to 30–40% overestimation. *Zhao et al*. [2009] examined subpixel cumulus contamination on MISR-retrieved AOD; for a few areas over the tropical oceans they examined the AOD at 558 nm wavelength was increased by about 0.02. One area over Indian Ocean, however, showed no increase in AOD despite over 10% of pixels containing some clouds. Overall, *Zhao et al*. [2009] argue that the climatology over tropical oceans is biased high by less than 0.002. Generally, direct cloud contamination might, in some way, be contributing to the observed MISR/OBS bias. The exact magnitude is difficult to assess. Regarding mitigation, implementing more sophisticated thin cirrus screening, for example, by utilizing MODIS-Terra long wavelengths in MISR processing, could possibly reduce this effect.

[37] The third line of reasoning mentioned above is the cloud adjacency effect. It is a complex three-dimensional and involving multiple scattering interaction of solar radiation between the clouds, surface, and surrounding environment [*Wen et al*., 2007; *Marshak et al*., 2008; *Wen et al*., 2008; *Yang and Di Girolamo*, 2008; *Kassianov et al*., 2009; *Várnai and Marshak*, 2009; *Davis and Marshak*, 2010; *Kassianov et al*., 2011]. An instructive graphical depiction of some of the interaction pathways can be found in *Yang and Di Girolamo* [2008]. Observational (based on MODIS) as well as conceptual studies indicate that cloud 3-D effects contribute substantially to the clear-sky radiance enhancement [*Wen et al*., 2007; *Yang and Di Girolamo*, 2008] and can bias satellite retrieved AODs for up to about 15 km away from clouds [*Várnai and Marshak*, 2009]. Some authors suggested a multispectral processing technique to partially correct for these effects [*Kassianov and Ovtchinnikov*, 2008; *Kassianov et al*., 2009]. Another option is to use conditional sampling, eliminating retrievals that could be affected by adjacent clouds. In principle, this is very similar to the analysis presented in this study, except that we use clear flag fraction instead of cloud fraction. These two are in fact highly correlated.

[38] It is important to notice that the cloud adjacency effects could only be a valid explanation if it gave rise to a differential effect between MISR and the Sun photometer. Indeed, any additional diffuse radiation reaching the Sun photometer would result in an AOD observation that is slightly smaller than the one resulting from the attenuation of direct

sunlight (Beer's law). This is in opposition to the satellite-based observations for which the cloud adjacency effects lead to increased AODs. Nevertheless, the impact of multiple scattered radiation on Sun photometer AODs is most likely negligible—we could not find studies addressing this issue. This suggests that the cloud adjacency effect is mostly pertinent to satellite-based observations.

[39] The choice of CFF instead of cloud-flag fraction is justified by a higher correlation coefficient (with the MISR/OBS bias reduction) in the case of CFF. The values are 0.29 and □ 0.43 for cloud-flag fraction and clear flag fraction, respectively, for the MISR/MAN data set. Clear flag fraction is more restrictive in a sense that it excludes subregions affected by glitter, clouds, cloud shadows, and all other pixels not satisfying strict quality criteria. Still, CFF is a less ambiguous metric; it furthermore accounts for the number of MISR cameras contributing to the retrieval. MISR multiangular observations substantially benefit retrieval quality, but less viewing angles can also introduce uncertainty. The fit to the aerosol scattering phase function is achieved best when all nine cameras are used. Therefore, higher CFFs are indicative of more accurate matching with the aerosol models used by MISR. This is obviously a simplification to the retrieval quality assessment, since retrievals are influenced by so many other factors. Even having nine cameras in a retrieval does not guarantee a perfect observation, as indicated by Figures 6 and 7.

5. Summary and Outlook

[40] In this study we present a simple procedure for reducing MISR AOD retrieval biases over dark water as compared to ground based MAN and AERONET observations. The method is based on the analysis of retrieval region characteristics specified by the Retrieval Applicability Masks reported in the MISR V22 data product. This subregion or subgrid scale information is used to filter out retrievals that are potentially contaminated by clouds or affected by cloud adjacency effects.

[41] Almost 1100 MISR/AERONET and 270 MISR/MAN collocations were identified; an increased number, as compared to previous studies, of MISR comparisons with ship-based MAN observations is particularly valuable. We found that MISR overestimates AODs, on average by 0.04, in reference to MAN, although the correlation coefficient (0.95) and RMSE (0.06) are slightly favorable relative to other comparison data sets. Furthermore, this positive bias can be substantially removed by employing the CFF (clear flag fraction) based screening procedure. An application of the CFF method to the multiyear global MISR dark water AOD data set reduced the average AOD from 0.15 to 0.12 (at CFF > 0.6).

[42] The 0.04 high bias in MISR AOD retrievals—as compared to MAN—can be a limiting factor for conducting research on aerosol dispersion and composition in more pristine marine conditions. In particular, it could hinder studies aimed at using satellite AOD retrievals for validating sea salt aerosol emission functions. For example, one outstanding problem is the existence of Southern Ocean AOD maximum, which is present in satellite records (MISR, MODIS, and SeaWIFS) and aerosol transport models, but is not yet evident in in situ MAN observations [*Smirnov et al.*, 2009, 2011]. In order to reconcile these different data sets, one has to consider possible satellite artifacts and biases as well as uncertainties in the sea salt production fluxes used in aerosol transport models. Furthermore, it is possible that MAN observations generally favor calmer environmental conditions when sea salt aerosol emission and concentrations are lower. The present study identifies MISR retrieval biases and offers a method for reducing them, which is a necessary step toward addressing the issue of Southern Ocean AOD maximum. This will be a subject of our future research, which will combine MISR retrievals and aerosol transport model simulations.

Appendix A: Cloud Screening Procedures in MISR Dark Water Aerosol Retrievals

[43] MISR uses three different metrics, or masks, to determine the presence of clouds, namely (1) the Radiometric Camera-by-camera Cloud Mask (RCCM), (2) the Angular Signature Cloud Mask (ASCM), and (3) the Stereoscopically Derived Cloud Mask (SDCM). The procedure differs depending on surface type; here only details regarding the deep water pathway will be described.

[44] The RCCM is calculated on camera-by-camera basis at 1.1 km resolution. Three RCCM designations are Cloud, Clear, and No Retrieval. (Note that in the Data Product Specification [*Bull et al.*, 2011] RCCM has five possible outcomes: ClearHC, ClearLC, CloudHC, CloudLC, and No Retrieval, where LC stands for low confidence and HC stands for high confidence. However, for the purpose of aerosol retrieval no differentiation between low confidence and high confidence is made, which effectively reduces the number of outcomes to three. Similar logic is applied to SDCM and ASCM products.) RCCM is constructed based on the bidirectional reflectance factor (BRF) in the near-IR band (866 nm, 1.1 km resolution) and the standard deviation of the 4 × 4 array of the red band (672 nm, 275 m resolution) BRFs within a 1.1 km area. The classification is achieved using a combination of threshold values that depend on Sun/viewing geometry. Details of the procedure can be found in *Diner et al.* [1999a] as well as in *Zhao and Di Girolamo* [2004]. Selecting the appropriate thresholds is a challenging problem, given the limited spectral information provided by MISR and the lack of spectral channels above 1 □m. Generally, the RCCM procedure has difficulties detecting thinner clouds, in particular thin cirrus clouds. For that reason, additional techniques have been applied to MISR cloud screening to alleviate this deficiency.

[45] The Angular Signature Cloud Mask (ASCM) is primarily based on a method developed by *Di Girolamo and Davies* [1994], called the Band-Differenced Angular Signature (BDAS) technique. This method is able to detect clouds, including thin cirrus, using a Rayleigh scattering signature at high forward-scattering angles. The BDAS technique uses the difference in BRF (□*R*) between band 1 (446 nm) and band 4 (866 nm) and examines this difference as a function of view angle [*Di Girolamo and Davies*, 1994; *Di Girolamo and Wilson*, 2003]. At high view angles and for clear scenes, □*R* increases due to enhanced contribution of Rayleigh scattering. However, in the presence of high clouds the Rayleigh contribution decreases, generating a strong signature in □*R* and enabling detection of such clouds. The BDAS technique uses primarily MISR cameras D and C (70.5° and 60.0°) in the

Table 5. Frequency of Flags Associated With Particular Tests in MISR Aerosol Processing for MISR/MAN Collocations[a]

Test Name	Retrieval Applicability Mask Flag Descriptions	Flag Frequency (%)
Cloud Masking (RCCM + ASCM + SDCM)	cloudy	13.2
Cloud Masking (RCCM + ASCM + SDCM)	cloudy other camera	2.3
Brightness	too bright	0.2
Brightness	bright other camera	0.1
Angle-to-angle Smoothness	not smooth	1.9
Angle-to-angle Correlation	not correlated	7.2

[a]The purpose of these tests is to detect clouds and other contaminations that could hinder aerosol retrievals. Acronyms are explained in the Appendix.

forward scattering direction (if BRF from either D or C camera is missing, camera B, 45.6°, is used instead). Some earlier sensitivity studies indicate that this method can detect thin cirrus clouds with optical depths as low as 0.5 [*Di Girolamo and Davies*, 1994]. Evaluation of the technique on real MISR data gives very satisfactory results [*Di Girolamo and Wilson*, 2003]. The resulting ASCM has —analogous to RCCM—three possible outcomes: Cloud, Clear, and No Retrieval.

[46] Finally, the Stereoscopically Derived Cloud Mask (SDCM) is a product of the stereo-matching technique used for cloud height retrieval [*Diner et al*., 1999b]. It is derived as a combination of the final stereoscopic height designator and RCCM. SDCM has the following outcomes: Cloud, NearSurface, and No Retrieval. For the purpose of aerosol retrieval, the "zero-wind" SDCM is used. This is because the actual heights are less important than the quality of cloud/no cloud discrimination.

[47] The three cloud masks—RCCM, ASCM, and SDCM —are combined to determine whether a particular 1.1 km subregion is clear or cloudy. Since each mask has three designators, a total of 27 combinations of flags are possible. The following rationale is used, grouped by the ASCM classification. If ASCM = No Retrieval then the subregion is designated cloudy, except for the case where SDCM has No Retrieval and RCCM is Clear, for which the subregion is designated as clear. This is motivated by the fact that in such situations most likely clear ocean is being observed. A Cloud designation from ASCM is sufficient to label the subregion as cloudy, regarding of RCCM or SDCM (this is possibly too conservative and requires testing). If ASCM = Clear the logic is similar to ASCM = No Retrieval, except that if SDCM returns NearSurface and RCCM is Clear, a clear designation is assigned. The assumption is that SDCM may be picking up thin, low smoke or dust aerosol plumes. In summary, out of 27 combinations of RCCM, ASCM, and SDCM flags, only three realizations are designated as clear: (ASCM, SDCM, RCCM) triads equal to (No Retrieval, No Retrieval, Clear), (Clear, No Retrieval, Clear), and (Clear, NearSurfac, Clear). This is quite a stringent approach, which assures that even the slightest indication of cloudiness in MISR radiances is sufficient to exclude the subregion from aerosol retrieval. Furthermore, the use of ASCM and the BDAS technique allows for excluding scenes with thin cirrus despite the lack of spectral channels above 1 □m.

[48] On top of the cloud masking procedure, three other tests are performed to eliminate pixels with cloud, glitter, and other contaminations that have escaped detection using other methods [*Diner et al*., 2008]. A simple brightness test is used to identify clouds that lacked texture necessary to be picked up by SDCM. If the BRFs of all spectral bands for any camera exceeded a threshold (set to 0.5), the subregion is eliminated from the retrieval. The additional two tests are the angle-to-angle smoothness test and the angle-to-angle correlation test.

[49] The angular smoothness test ensures that the equivalent reflectance field is "smooth" as a function of angle. It is applied to each spectral band separately, and to the forward (+nadir) camera set independently of the aftward (+nadir) camera set. For each camera set, a polynomial is fitted to the subregion equivalent reflectances; the order of the polynomial is 1° less than the number of cameras (4th order for five cameras and 3rd order for four cameras). The goodness of fit is then calculated with a χ^2 test (for details see *Diner et al*. [2008]). If the value of χ^2 exceeds 4, then the subregion is eliminated from aerosol processing.

[50] The angle-to-angle correlation test uses subpixel information from the 275 m red band data. It examines each camera and detects suspicious features in the subpixel equivalent reflectances. Those suspicious features might arise from small clouds undetected by the standard cloud masks, and could lead to a higher than expected variance of equivalent reflectances within a 1.1 km subregion. First, a 4×4 image template is constructed by averaging red band data (275 m resolution) over all camera angles. Then the variance of the template image is calculated using the radiances from four subpixels. Next step is to calculate, for each camera, the variance for an actual camera image and the covariance between the camera image and the template image. Then the normalized cross-correlation is calculated using the above variances and covariances (see *Diner et al.* [2008] for details). If the cross correlation for a particular camera is lower than a certain threshold (set to 0.25), the whole subregion is eliminated from aerosol processing.

[51] It would be instructive to examine frequencies with which each test identifies cloudy subregions, which would shows how effective the tests are and which one is most useful in finding contaminated pixels. Such an analysis, however, is impossible due to sequential nature of processing—if one test fails for a particular camera or subregion, subsequent tests are never performed. Despite that, some qualitative information about cloud clearing performance could be extracted by analyzing Retrieval Applicability Mask flag values and their frequencies. These frequencies are calculated from 270 MISR/MAN comparison points for all regions within the 30 km perimeter from the MAN location; all regions are considered regardless of whether there was a valid retrieval or not. In total there are 2454 regions, of which 1451 have successful retrievals. The frequencies of each flag are presented in Table 5. Note that the order in which the tests are applied influences flag frequencies—in aerosol processing test execution is the following: cloud masking, brightness

test, angular smoothness test, and angular correlation test. Cloud masking eliminates about 15.5% (cloudy + cloudy other camera) subregions that have passed previous quality control checks. The brightness test has very small percentage of failures, indicating that the preceding cloud masking eliminates most of the bright pixels. Out of the two angular tests, the angle-to-angle correlation test is more effective than the smoothness test. Clearly, higher resolution data from the red band add additional sensitivity and prove highly effective in identifying cloud and other contaminations that escaped previous tests.

[52] The above listed procedures identify contaminated or cloudy pixels and eliminate them from the aerosol retrievals. It is expected that clouds with optical depths as low as 0.1 to 0.5 are detected and screened for (L. Di Girolamo, personal communication, 2013). The actual threshold depends on Sun-view geometry, the structure of the cloud, whether the cloud is ice or liquid, and the amount of aerosols above and below the cloud. A study evaluating the performance of cloud screening procedures for aerosol retrieval purposes is in preparation.

[53] **Acknowledgments.** We thank the PIs and their staff for establishing and maintaining the 19 AERONET sites used in this investigation. We acknowledge the MAN program principal investigators and their staff for providing the data. We also thank three anonymous reviewers for their useful comments and criticism. The research was carried out at the Jet Propulsion Laboratory, California Institute of Technology, under a contract with the National Aeronautics and Space Administration.

References

Bull, M., J. Matthews, D. McDonald, A. Menzies, C. Moroney, K. Mueller, S. Paradise, and M. Smyth (2011), MISR data product specification, Jet Propulsion Laboratory, JPL D-13963, Rev. S, 324 pp. [Available online at https://eosweb.larc.nasa.gov/sites/default/files/project/misr/DPS_v50_RevS.pdf].

Davis, A. B., and A. Marshak (2010), Solar radiation transport in the cloudy atmosphere: A 3D perspective on observations and climate impacts, *Rep. Prog. Phys.*, *73*, 026801, doi:10.1088/0034-4885/73/2/026801.

De Leeuw, G., E. L. Andreas, M. D. Anguelova, C. W. Fairall, E. R. Lewis, C. O'Dowd, M. Schulz, and S. E. Schwartz (2011), Production flux of sea spray aerosol, *Rev. Geophys.*, *49*, RG2001, doi:10.1029/2010RG000349.

Dey, S., and L. Di Girolamo (2010), A climatology of aerosol optical and microphysical properties over the Indian subcontinent from 9 years (2000–2008) of Multiangle Imaging Spectroradiometer (MISR) data, *J. Geophys. Res.*, *115*, D15204, doi:10.1029/2009JD013395.

Di Girolamo, L., and M. J. Wilson (2003), A first look at band-differenced angular signatures for cloud detection from MISR, *IEEE Trans. Geosci. Remote Sens.*, *41*(7), 1730–1734, doi:10.1109/TGRS.2003.815659.

Di Girolamo, L., and R. Davies (1994), A band-differenced angular signature technique for cirrus cloud detection, *IEEE Trans. Geosci. Remote Sens.*, *32*(4), 890–896.

Diner, D. J., L. Di Girolamo, and E. Clothiaux (1999a), MISR level 1 cloud detection algorithm theoretical basis. Jet Propulsion Laboratory, JPL D-13397, Rev. B, 38 pp. [Available online at http://eospso.gsfc.nasa.gov/sites/default/files/atbd/atbd-misr-06.pdf].

Diner, D. J., R. Davies, L. Di Girolamo, A. Horvath, C. Moroney, J.-P. Muller, S. R. Paradise, D. Wenkert, and J. Zong (1999b), MISR level 2 cloud detection and classification algorithm theoretical basis. Jet Propulsion Laboratory, JPL D-11399, Rev. D, 102 pp. [Available online at http://eospso.gsfc.nasa.gov/sites/default/files/atbd/atbd-misr-07.pdf].

Diner, D. J., et al. (2008), MISR level 2 aerosol retrieval algorithm theoretical basis. Jet Propulsion Laboratory, JPL D-11400, Rev. G, 81 pp. [Available online at http://eospso.gsfc.nasa.gov/sites/default/files/atbd/atbd-misr-09.pdf].

Eck, T. F., B. N. Holben, J. S. Reid, O. Dubovik, A. Smirnov, N. T. O'Neill, I. Slutsker, and S. Kinne (1999), Wavelength dependence of the optical depth of biomass burning, urban, and desert dust aerosols, *J. Geophys. Res.*, *104*, 31,333–31,349.

Holben, B. N., et al. (1998), AERONET—A federated instrument network and data archive for aerosol characterization, *Remote Sens. Environ.*, *66*, 1–16.

Holben, B. N., et al. (2001), An emerging ground-based aerosol climatology: Aerosol optical depth from AERONET, *J. Geophys. Res.*, *106*, 12,067–12,097.

IPCC (Intergovernmental Panel on Climate Change) (2001), Radiative forcing of climate change, in *Climate Change 2001*, Cambridge Univ. Press, New York.

IPCC (Intergovernmental Panel on Climate Change) (2007), The physical science basis, in *Contribution of Working Group I to the Fourth Assessment Report of the Intergovernmental Panel on Climate Change*, edited by S. Solomon et al., pp. 996, Cambridge Univ. Press, New York.

Jeong, M.-J., and Z. Li (2010), Separating real and apparent effects of cloud, humidity, and dynamics on aerosol optical thickness near cloud edges, *J. Geophys. Res.*, *115*, D00K32, doi:10.1029/2009JD013547.

Kahn, R. A. (2012), Reducing the uncertainties in direct aerosol radiative forcing, *Surv. Geophys.*, *33*, 701–721, doi:10.1007/s10712-011-9153.

Kahn, R. A., B. Gaitley, J. Martonchik, D. Diner, K. Crean, and B. Holben (2005a), MISR global aerosol optical depth validation based on two years of coincident AERONET observations, *J. Geophys. Res.*, *110*, D10S04, doi:10.1029/2004JD004706.

Kahn, R. A., W.-H. Li, J. V. Martonchik, C. J. Bruegge, D. J. Diner, B. J. Gaitley, and W. Abdou (2005b), MISR calibration and implications for low-light-level aerosol retrieval over dark water, *J. Atmos. Sci.*, *62*, 1032–1062.

Kahn, R. A., M. J. Garay, D. L. Nelson, K. K. Yau, M. A. Bull, B. J. Gaitley, J. V. Martonchik, and R. C. Levy (2007), Satellite-derived aerosol optical depth over dark water from MISR and MODIS: Comparisons with AERONET and implications for climatological studies, *J. Geophys. Res.*, *112*, D18205, doi:10.1029/2006JD008175.

Kahn, R. A., D. L. Nelson, M. J. Garay, R. C. Levy, M. A. Bull, D. J. Diner, J. V. Martonchik, S. R. Paradise, E. G. Hansen, and L. A. Remer (2009), MISR aerosol product attributes and statistical comparison with MODIS, *IEEE Trans. Geosci. Remote Sens.*, *47*, 4095–4114.

Kahn, R. A., B. J. Gaitley, M. J. Garay, D. J. Diner, T. F. Eck, A. Smirnov, and B. N. Holben (2010), Multiangle Imaging SpectroRadiometer global aerosol product assessment by comparison with the Aerosol Robotic Network, *J. Geophys. Res.*, *115*, D23209, doi:10.1029/2010JD014601.

Kahn, R. A., M. J. Garay, D. L. Nelson, R. C. Levy, M. A. Bull, D. J. Diner, J. V. Martonchik, E. G. Hansen, L. A. Remer, and D. Tanré (2011), Response to "Toward unified satellite climatology of aerosol properties. 3. MODIS versus MISR versus AERONET", *J. Quant. Spectros. Radiat. Transfer*, *112*, 901–909, doi:10.1016/j.jqsrt.2009.11.003.

Kassianov, E. I., and M. Ovtchinnikov (2008), On reflectance ratios and aerosol optical depth retrieval in the presence of cumulus clouds, *Geophys. Res. Lett.*, *35*, L06807, doi:10.1029/2008GL033231.

Kassianov, E. I., M. Ovchinnikov, L. K. Berg, S. A. McFarlane, and C. Flynn (2009), Retrieval of aerosol optical properties in vicinity of broken clouds from reflectance ratios: Sensitivity study, *J. Quant. Spectros. Rad. Trans.110*, 1677–1689.

Kassianov, E. I., M. Ovchinnikov, L. K. Berg, and C. Flynn (2011), Conventional clear-sky aerosol retrievals: Do they work for cloudy days?, Atti Accad. Pelorit. Pericol. Cl. Sci. Fis. Mat. Nat., 89, Suppl. No. 1, C1V89S1P047, doi:10.1478/C1V89S1P047.

Kaufman, Y. J., L. A. Remer, D. Tanré, R.-R. Li, R. Kleidman, S. Mattoo, R. C. Levy, T. F. Eck, B. N. Holben, and C. Ichoku (2005), A critical examination of the residual cloud contamination and diurnal sampling effects on MODIS estimates of aerosol over ocean *IEEE Trans. Geosci. Remote Sens.*, *43*(12), 2886–2897.

Knobelspiesse, K. D., C. Pietras, G. S. Fargion, M. H. Wang, R. Frouin, M. A. Miller, S. Subramaniam, and W. M. Balch (2004), Maritime aerosol optical thickness measured by handheld sunphotometers, *Remote Sens. Environ.*, *93*, 87–106.

Koren, I., L. A. Remer, Y. J. Kaufman, Y. Rudich, and J. V. Martins (2007), On the twilight zone between clouds and aerosols, *Geophys. Res. Lett.*, *34*, L08805, doi:10.1029/2007GL029253.

Lallart, P., R. A. Kahn, and D. Tanré (2008), POLDER2/ADEOSII, MISR, and MODIS/Terra reflectance comparison, *J. Geophys. Res.*, *113*, D14S02, doi:10.1029/2007JD009656.

Li, Z., X. Zhao, R. Kahn, M. Mishchenko, L. Remer, K.-H. Lee, M. Wang, I. Laszlo, T. Nakajima, and H. Maring (2009), Uncertainties in satellite remote sensing of aerosols and impact on monitoring its long-term trend: A review and perspective, *Ann. Geophys.*, *27*, 2755–2770.

Liu, L., and M. I. Mishchenko (2008), Toward unified satellite climatology of aerosol properties: Direct comparison of advanced level 2 aerosol products, *J. Quant. Spectros. Radiat. Transfer*, *109*, 2376–2385, doi:10.1016/j.jqsrt.2008.05.003.

Lyapustin, A., Y. Wang, R. A. Kahn, J. Xiong, A. Ignatov, R. Wolfe, A. Wu, B. Holben, and C. Bruegge (2007), Analysis of MODIS–MISR calibration differences using surface albedo around AERONET sites and cloud reflectance, *Remote Sens. of Environ.*, *107*, 12–21, doi:10.1016/j.rse.2006.09.028.

Marshak, A., G. Wen, J. A. Coakley Jr., L. A. Remer, N. G. Loeb, and R. F. Cahalan (2008), A simple model for the cloud adjacency effect and the apparent bluing of aerosols near clouds, *J. Geophys. Res.*, *113*, D14S17, doi:10.1029/2007JD009196.

Martonchik, J. V., D. J. Diner, R. A. Kahn, B. J. Gaitley, and B. N. Holben (2004), Comparison of MISR and AERONET aerosol optical depth over desert sites, *Geophys. Res. Lett.*, *31*, L16102, doi:10.1029/2004GL019807.

Mishchenko, M. I., I. V. Geogdzhayev, W. B. Rossow, B. Cairns, B. E. Carlson, A. A. Lacis, L. Liu, and L. D. Travis (2007), Long-term satellite record reveals likely recent aerosol trend, *Science*, *315*, 1,543, doi:10.1126/science.1136709.

Mishchenko, M. I., L. Liu, I. V. Geogdzhayev, L. D. Travis, B. Cairns, and A. A. Lacis (2010), Toward unified satellite climatology of aerosol properties 3. MODIS versus MISR versus AERONET, *J. Quant. Spectros. Radiat. Transfer*, *111*, 540–552, doi:10.1016/j.jqsrt.2009.11.003.

MISR Data Product Specification (2011), JPL D-13963, Revision S.

Porter, J. N., M. Miller, C. Pietras, and G. Motell (2001), Ship-based sun photometer measurements using microtops sun photometers, *J. Atmos. Oceanic Technol.*, *18*, 765–774.

Quass, J., O. Boucher, N. Bellouin, and S. Kinne (2008), Satellite-based estimate of the direct and indirect aerosol climate forcing, *J. Geophys. Res.*, *113*, D05204, doi:10.1029/2007JD008962.

Redemann, J., Q. Zhang, P. B. Russell, J. M. Livingston, and L. A. Remer (2009), Case studies of aerosol remote sensing in the vicinity of clouds, *J. Geophys. Res.*, *114*, D06209, doi:10.1029/2008JD010774.

Remer, L. A., et al. (2005), The MODIS aerosol algorithm, products and validation, *J. Atmos. Sci.*, *62*, 947–973, doi:10.1175/JAS3385.1.

Remer, L. A., et al. (2008), Global aerosol climatology from the MODIS satellite sensors, *J. Geophys. Res.*, *113*, D14S07, doi:10.1029/2007JD009661.

Sayer, A. M., N. C. Hsu, C. Bettenhausen, Z. Ahmad, B. N. Holben, A. Smirnov, G. E. Thomas, and J. Zhang (2012), SeaWiFS Ocean Aerosol Retrieval (SOAR): Algorithm, validation, and comparison with other data sets, *J. Geophys. Res.*, *117*, D03206, doi:10.1029/2011JD016599.

Schwartz, S. E., R. J. Charlson, R. A. Kahn, J. A. Ogren, and H. Rodhe (2010), Why hasn't Earth warmed as much as expected?, *J. Clim.*, *23*, 2453–2464, doi:10.1175/2009JCLI3461.

Shi, Y., J. Zhang, J. S. Reid, B. Holben, E. J. Hyer, and C. Curtis (2011a), An analysis of the collection 5 MODIS over-ocean aerosol optical depth product for its implication in aerosol assimilation, *Atmos. Chem. Phys.*, *11*, 557–565, doi:10.5194/acp-11-557-2011.

Shi, Y., J. Zhang, J. S. Reid, E. J. Hyer, T. F. Eck, B. N. Holben, and R. A. Kahn (2011b), A critical examination of spatial biases between MODIS and MISR aerosol products—Application for potential AERONET deployment, *Atmos. Meas. Tech.*, *4*, 2823–2836, doi:10.5194/amt-4-2823-2011.

Smirnov, A., B. N. Holben, A. Lyapustin, I. Slutsker, and T. F. Eck (2004), AERONET processing algorithm refinement, AERONET workshop, El Arenosillo, Spain, 10–14 May 2004.

Smirnov, A., et al. (2006), Ship-based aerosol optical depth measurements in the Atlantic Ocean: Comparison with satellite retrievals and GOCART model, *Geophys. Res. Lett.*, *33*, L14817, doi:10.1029/2006GL026051.

Smirnov, A., et al. (2009), Maritime Aerosol Network as a component of Aerosol Robotic Network, *J. Geophys. Res.*, *114*, D06204, doi:10.1029/2008JD011257.

Smirnov, A., et al. (2011), Maritime aerosol network as a component of AERONET—First results and comparison with global aerosol models and satellite retrievals, *Atmos. Meas. Tech.*, *4*, 583–597.

Su, W., G. L. Schuster, N. G. Loeb, R. R. Rogers, R. A. Ferrare, C. A. Hostetler, J. W. Hair, and M. D. Obland (2008), Aerosol and cloud interaction observed from high spectral resolution lidar data, *J. Geophys. Res.*, *113*, D24202, doi:10.1029/2008JD010588.

Toth, T. D., J. Zhang, J. R. Campbell, J. S. Reid, Y. Shi, R. S. Johnson, A. Smirnov, M. A. Vaughan, and D. M. Winker (2013), Investigating enhanced Aqua MODIS aerosol optical depth retrievals over the mid-to-high latitude Southern Oceans through intercomparison with co-located CALIOP, MAN, and AERONET data sets, *J. Geophys. Res. Atmos.*, *118*, 4700–4714, doi:10.1002/jgrd.50311.

Twohy, C. H., J. A. Coakley Jr., and W. R. Tahnk (2009), Effect of changes in relative humidity on aerosol scattering near clouds, *J. Geophys. Res.*, *114*, D05205, doi:10.1029/2008JD010991.

Várnai, T., and A. Marshak (2009), MODIS observations of enhanced clear sky reflectance near clouds, *Geophys. Res. Lett.*, *36*, L06807, doi:10.1029/2008GL037089.

Várnai, T., and A. Marshak (2011), Global CALIPSO observations of aerosol changes near clouds, *IEEE Geosci. Remote Sens. Lett.*, *8*(1), 19–23.

Wen, G., A. Marshak, R. F. Cahalan, L. A. Remer, and R. G. Kleidman (2007), 3-D aerosol-cloud radiative interaction observed in collocated MODIS and ASTER images of cumulus cloud fields, *J. Geophys. Res.*, *112*, D13204, doi:10.1029/2006JD008267.

Wen, G., A. Marshak, and R. F. Cahalan (2008), Importance of molecular Rayleigh scattering in the enhancement of clear sky reflectance in the vicinity of boundary layer cumulus clouds, *J. Geophys. Res.*, *113*, D24207, doi:10.1029/2008JD010592.

Wild, M. (2009), Global dimming and brightening: A review, *J. Geophys. Res.*, *114*, D00D16, doi:10.1029/2008JD011470.

Yang, Y., and L. Di Girolamo (2008), Impacts of 3-D radiative effects on satellite cloud detection and their consequences on cloud fraction and aerosol optical depth retrievals, *J. Geophys. Res.*, *113*, D04213, doi:10.1029/2007JD009095.

Yu, H., et al. (2006), A review of measurement-based assessment of aerosol direct radiative effect and forcing, *Atmos. Chem. Phys.*, *6*, 613–666.

Zhang, J., and J. S. Reid (2006), MODIS aerosol product analysis for data assimilation: Assessment of over-ocean level 2 aerosol optical thickness retrievals, *J. Geophys. Res.*, *111*, D22207, doi:10.1029/2005JD006898.

Zhang, J., and J. S. Reid (2010), A decadal regional and global trend analysis of the aerosol optical depth using a data-assimilation grade over-water MODIS and Level 2 MISR aerosol products, *Atmos. Chem. Phys.*, *10*, 10,949–10,963, doi:10.5194/acp-10-10949-2010.

Zhang, J., J. S. Reid, and B. N. Holben (2005), An analysis of potential cloud artifacts in MODIS over ocean aerosol thickness products, *Geophys. Res. Lett.*, *32*, L15803, doi:10.1029/2005GL023254.

Zhao, G., and L. Di Girolamo (2004), A cloud fraction versus view angle technique for automatic in-scene evaluation of the MISR cloud mask, *J. Appl. Meteorol.*, *43*, 860–869.

Zhao, G., L. Di Girolamo, S. Dey, A. L. Jones, and M. Bull (2009), Examination of direct cumulus contamination on MISR-retrieved aerosol optical depth and angstrom coefficient over ocean, *Geophys. Res. Lett.*, *36*, L13811, doi:10.1029/2009GL038549.